Bioprinting 41 (2024) e00348

Contents lists available at ScienceDirect

Bioprinting

journal homepage: www.sciencedirect.com/journal/bioprinting

Diffusion coefficients in scaffolds made with temperature controlled cryoprinting and an ink made of sodium alginate and agar

Leo Lou [a,*], Boris Rubinsky [a,b]

[a] Department of Bioengineering, University of California Berkeley, Berkeley, CA, 94720, USA
[b] Department of Mechanical Engineering, University of California Berkeley, Berkeley, CA, 94720, USA

ARTICLE INFO

Keywords:
Temperature Controlled Cryoprinting(TCC)
Modified diffusion coefficient
Anisotropic diffusion

ABSTRACT

Temperature Controlled Cryoprinting (TCC), is a tissue engineering technique wherein each deposited voxel is frozen with precise control over cooling rates and the direction of freezing. This control allows for the generation of ice crystals with controlled shape and orientation. Recently we found that the macroscale fidelity of the TCC print is substantially improved by using a 3D printing ink composed of a mixture of two compounds: one that solidifies through chemical crosslinking (sodium alginate) and another that solidifies through physical (thermal) effects (agar). In this study we examine the hypothesis that the combination of sodium alginate and agar, affects also the fidelity of the microstructure and thereby the diffusivity of the scaffold. The ability of this technology to generate controlled diffusivity within the tissue scaffold was examined with a directional solidified TCC sample using fluorescence recovery after photobleaching (FRAP) and scanning electron microscope (SEM). We find that the diffusion coefficient in $m^2/s \times 10^{-10}$ is: 1.62 ± 1.27 for the unfrozen sample, 2.40 ± 1.54 for the rapidly frozen sample and 9.72 ± 4.50 for the slow frozen sample. This points to two conclusions. One is that the diffusivity is slow frozen samples is higher than that in unfrozen samples and in rapidly frozen sample. A second observation is that a relatively narrow range of diffusivity variance was obtained when using 2%w/v sodium alginate and 2%w/v of agar. However, when the concentration of agar was reduced to 0.5w/v a much wider spread of diffusivities was measure, 4.07 ± 1.65. This suggests that the addition of agar has also an effect on the microscale fidelity, and consequently the diffusivity. The anisotropic diffusion properties of TCC-printed directional solidification samples were also validated through both FRAP and SEM.

1. Introduction

In tissue engineering, tissue scaffolds are designed to provide a supportive framework for cells to adhere, proliferate, and ultimately generate new tissue. While scaffolds can be fashioned from diverse materials, they must exhibit certain essential attributes: biocompatibility and appropriate physical, chemical, mechanical, and structural properties [1]. A critical factor in tissue engineering is the scaffold's capability to facilitate nutrient and waste transport.

Transport within a scaffold depends on diffusion and convection. Diffusion plays a pivotal role in transporting nutrients and waste across different tissues like the liver and cartilage, traversing the extracellular matrix. Given its significance as a transport mechanism, attention must be paid to designing the diffusion characteristics of the scaffold. The challenges associated with oxygen and nutrient delivery, waste elimination, protein migration, and cell movement are fundamentally shaped by the scaffold's diffusion coefficient, which is intricately linked to the scaffold microstructure [2–4].

The research presented in this paper stems from an exploration of our 3D bioprinting technology known as Temperature Controlled Cryoprinting (TCC) [5,6]. A fundamental aspect of TCC is the precise freezing of each individual deposited voxel, maintaining a controlled temperature history throughout the entire 3D printed structure [5,6]. In TCC, the cooling rates during the freezing of each voxel are meticulously regulated by controlling factors such as the temperature of the printing fluid, the temperature of the last printed layer, and the energy balance on each voxel during deposition [7,8]. Our research group has developed a range of TCC techniques aimed at precisely controlling the temperature history during the freezing of each individual voxel [5–9], [10–12].

Other tissue engineering techniques utilize freezing as well. For instance, in one category of freezing methods for 3D printing, the chamber surrounding the printing system maintains subfreezing

* Corresponding author.
E-mail address: taolou@berkeley.edu (L. Lou).

https://doi.org/10.1016/j.bprint.2024.e00348
Received 26 April 2024; Received in revised form 7 June 2024; Accepted 13 June 2024
Available online 15 June 2024

temperatures, with precise control over the chamber temperature [13]. Another technique involves freezing to create tissue strands, deposited in a manner that facilitates the formation of pores between the strands [14]. Many techniques maintain the printing surface at a constant sub-freezing temperature [15–17]. However, a drawback of these "static" methods is that cooling rates during freezing vary depending on the distance from the printing plate, decreasing as the distance increases. The unique feature of TCC (Temperature Controlled Cryo-printing) lies in its ability to freeze each voxel at controlled temperatures, enabling precise control over the microstructure of ice crystals throughout the entire printed structure [7,8]. Recently, other research groups [18] have adopted elements of our work on TCC, such as controlled freezing of each voxel [5,6], multi-layered freezing [11], cross-linking during thawing [19], and freezing with optimal thermal parameters for cell survival [20].

The TCC technology provides several advantages over conventional 3D bioprinting [5,6,11,12]:

A) Materials utilized in tissue engineering typically possess soft characteristics, posing challenges in the printing of large and intricate structures. Nevertheless, with the freezing of each voxel upon deposition, the freezing process enhances the mechanical strength of the printed scaffold. This enhancement enables the creation of intricately large and complex structures.
B) Traditional 3D bioprinting procedures can be lengthy, and organic matter used in the process may deteriorate over time. However, in TCC, the printed material remains frozen from deposition until the printing of the entire object is completed. Consequently, there is no risk of deterioration during printing, regardless of the time required to print the object.
C) It is anticipated that in the future, printed organs will be cryopreserved prior to transplantation, especially when the printing facility is located a considerable distance from the transplantation site. Through the controlled freezing of each voxel, TCC 3D cryoprinting ensures that the printed item is preserved in a frozen state immediately during the printing, facilitating transportation in a cryopreserved state. This capability was demonstrated in a recent study [19,20].
D) Temperature control during the freezing of each voxel enables the implementation of an optimal cryopreservation protocol for the cells within each voxel. This ensures that cells throughout the entire structure survive cryopreservation, regardless of the size of the printed object [20].
E) Most pertinent to this paper is the realization that the microstructure of the printed scaffold is determined by the ice crystal structure formed during freezing. Through meticulous control of the temperature history during the freezing of each voxel, it becomes feasible to regulate the ice crystal structure at the microscale within each voxel. This temperature control during freezing enables TCC to generate finely regulated ice microstructures within every voxel of the bio-scaffold, offering unparalleled precision in this aspect [10]' [8,11,12,21,22].

In our research on the TCC technology, we have also addressed challenges related to printability requirements. In 3D printing, a significant obstacle arises from the need to balance conflicting demands on the properties of the printing ink during delivery and deposition phases. During delivery, the ink benefits from low viscosity and high fluidity, whereas upon deposition, it must solidify instantly. Typically, the ink comprises hydrocolloids in an aqueous solution, solidifying through crosslinking achieved by two main methods: a) Chemical crosslinking, such as ionically crosslinking alginate with $CaCl_2$. b) Physical crosslinking, exemplified by agar, which solidifies at room temperature [8,11,12,21,22].

In our study, alginate serves as the primary hydrocolloid. Alginate is widely employed in tissue engineering [23,24] due to its favorable properties. However, its crosslinking poses a challenge. The crosslinking process involves a time-dependent diffusion process. If crosslinking occurs before deposition, it substantially increases the viscosity of the solution in the printing nozzle. On the other hand, if crosslinking happens after deposition, it may take too long and result in structural collapse. Currently, various technologies are under development to address these challenges. These technologies involve compromises in terms of different combinations of alginate and crosslinking, taking into account timing and the amount of crosslinker delivered.

We have approached this challenge differently using the TCC technology. In our method, the ink is delivered without any crosslinker, and the material freezes upon deposition, providing the rigidity that would typically result from crosslinking. Subsequently, the frozen sample is immersed in a bath of crosslinker and melted, with precise temperature control ensuring that the melting interface progresses in tandem with the diffusion of the crosslinker, starting from the exterior and moving inward. This approach allows the rigidity provided by freezing to be replaced by that of the crosslinked material, while the object remains frozen and rigid until it is melted and crosslinked. Our successful demonstration of this technology in a study illustrated its capability to simultaneously print and cryopreserve living cells that survive the process [19,20].

We recently introduced a modification to the TCC procedure [25], which serves as the basis for this paper. This modification specifically addresses the issue of alginate prints shrinking upon crosslinking, which adversely affects print fidelity [19]. Our inspiration for this modification stemmed from observations in dentistry dating back to the early 20th century, where agar was commonly added to alginate to create high-fidelity teeth implants [26]. More recently, the combination of agar and alginate has been utilized in drug delivery [27] applications. This combination of crosslinked alginate and agar has also been applied in 3D printing to mitigate the Barus effect in the printing head fluid [28].

Our study has demonstrated that the addition of agar significantly improves print fidelity, with the extent of enhancement being dependent on the relative agar concentration [25]. However, we believe that the addition of agar has another important effect in TCC printing. Our hypothesis posits that in TCC printing of a combination of agar and alginate, a specific process occurs. Initially, an ink comprising warm agar and uncrosslinked alginate exhibits high fluidity. Upon deposition on a cold surface, as the temperature of the voxel decreases from room temperature towards freezing, the agar in each voxel rapidly undergoes physical crosslinking at temperatures above freezing, providing temporary rigidity, while the alginate remains uncrosslinked. Subsequently, as the temperature of the voxel decreases further below the freezing point, the entire voxel, including the uncrosslinked alginate and the crosslinked agar, freezes. During the subsequent steps of TCC, such as crosslinking upon thawing by immersion in a bath of $CaCl_2$[19], a unique attribute of an ink made of a combination of agar and alginate may emerge. We think that the addition of the agar should affect print fidelity at both the macroscale and the microscale. This should affect diffusivity. To test this hypothesis, we conducted a study on the diffusion coefficient of TCC-printed objects, varying agar concentration and freezing rates. This was accomplished using Fluorescent Recovery After Photobleaching (FRAP) [29].

Our research validated the concept that employing temperature-controlled cryoprinting with an ink composed of alginate and agar could effectively regulate and improve scaffold diffusivity. In future studies, we aim to integrate cell tests to further elucidate the relationship between anisotropic diffusivity and cellular behavior.

2. Materials and methods

2.1. Ink preparation

To prepare the gel solution, Agar (Sigma-Aldrich, St. Louis, MO, USA) and sodium alginate (Sigma-Aldrich, St. Louis, MO, USA) were

dissolved in deionized (DI) water. The DI water was heated to 100 °C using a heating plate (Corning Inc., Somerville, MA, USA) to dissolve the agar and sodium alginate powders completely. Once all the powder was dissolved, the solution was cooled to 40 °C.

The study involved two compositions:

1. 2 % Sodium Alginate/2 % Agar w/w (2 % SA/2 % AG)
2. 2 % Sodium Alginate/0.5 % Agar w/w (2 % SA/0.5 % AG)

2.2. TCC printing system

For this study, we developed and constructed a temperature-controlled 3D cryoprinting (TCC) system. The printing component of the system was adapted from an Ender 3 3D Printer, manufactured by Shenzhen Creality in Shenzhen, China. The printing syringe was filled with the mixed hydrogel, and its temperature was maintained at 40 °C before printing. During printing, the extrusion syringe was equipped with a flexible heater from Omega, based in Norwalk, New Jersey. This heater was utilized to keep the syringe's temperature at 40 °C, ensuring proper material flow and preventing unwanted gelation.

Printing occurred on a constantly cooled surface maintained at +4 °C, achieved through a connected cooling bath provided by Polyscience Inc., located in Phoenix, AZ. The cooling bath utilized a mixture of 50 % ethanol and 50 % water to maintain a temperature of +4 °C during the initial printing step.

In this study, a 2 cm by 2 cm by 0.1 cm printed object was used. Cooling to +4 °C facilitated the physical crosslinking of the agar, providing rigidity to the entire structure, while the alginate remained in a liquid state.

2.3. Freezing

The printed sample underwent freezing using directional solidification, as illustrated in Fig. 1. A cooling bath containing 5 % ethylene glycol was set to −25 °C, and the sample was immersed into the cooling bath along its long axis with a constant velocity controlled by a syringe pump motor. The temperature and freezing velocity were adjusted to achieve two different freezing rates: slow freezing (SF) with a freezing rate of 5 °C/min and rapid freezing (RF) with a freezing rate of 25 °C/min. Directional solidification facilitates freezing with controlled cooling rates of every voxel in the structure.

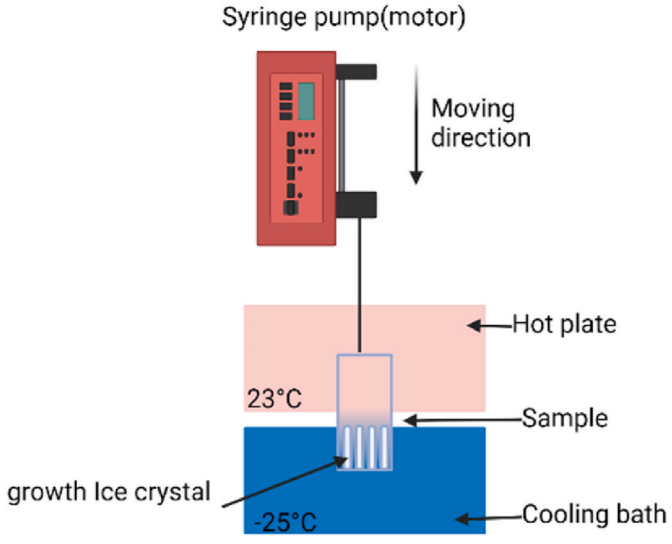

Fig. 1. Directional Solidification Setup: The diagram illustrates a schematic depiction of the directional solidification apparatus. It includes a cooling bath filled with a solution containing 5 % ethylene glycol. The sample intended for freezing (ice crystals formation) is submerged into the cooling bath along its longitudinal axis, with its movement regulated by a syringe pump motor to maintain a constant velocity. An arrow indicates the direction of the sample movement. Two distinct freezing rates, referred to as slow freezing (SF) and rapid freezing (RF), are achieved by adjusting the temperature and freezing velocity accordingly.

2.4. Crosslinking

After freezing, all samples underwent crosslinking, following the same procedure outlined in our previous study. This process typically involved immersing the samples in a 2 % $CaCl_2$ solution (Fisher Scientific, Fairlawn, NJ, USA) for 15 min at room temperature. Following crosslinking, the samples were prepared for fluorescent dyeing. As controls, we also included a sample that was not frozen (NF). The NF sample did not undergo directional freezing and was crosslinked immediately after it was printed, at 4 °C.

2.5. Fluorescent dye

In preparation for the fluorescence test, the cross-linked scaffold was immersed in a 1 mol/ m^3 fluorescein solution for 20 h. The 1 mol/ m^3 fluorescein solution was prepared by dissolving 0.033g of Fluorescein (Sigma-Aldrich, St. Louis, MO) in 100 ml of DI water. It is noteworthy that our previous study demonstrated that agar/alginate samples made by TCC maintained their shape for such extended periods under liquid exposure conditions [25].

2.6. Fluorescent recovery after photobleaching (FRAP)

Fluorescence Recovery After Photobleaching (FRAP) is a method utilized for analyzing the movement and interactions of large molecules within a sample [29]. The process involves directing a powerful laser pulse at the fluorescence wavelength to a specific area of the sample, inducing a structural change in the fluorescent molecules within that zone, thus preventing them from emitting light. Consequently, this area becomes dark. Over time, the darkened region begins to brighten again as unaltered fluorescent molecules migrate into the space, allowing for the observation of molecular diffusion dynamics. By examining the rate at which fluorescence returns, we can determine both the diffusion rates of molecules and the proportion of molecules that are able to move freely within the sample.

The test sample comprised a 1 cm diameter cylinder with a thickness of 1 mm, obtained from the square scaffold (2 cm * 2 cm * 1 mm) fabricated as described earlier (Fig. 2). The FRAP test was conducted using the Zeiss LSM880 FCS at room temperature. During the FRAP test, a 488 nm laser was utilized to bleach the target field, specifically a 250 μm diameter circle. A total of 150 image frames were collected, with 10 frames captured before bleaching and 140 frames taken during the recovery phase after bleaching. The bleach and recovery process extended for 60 s (Fig. 3). Each testing group consisted of 5 repeated experiments.

2.7. Experimental groups

The study investigates four experimental groups to assess the impact of freezing rate, agar concentration, and directional solidification on the measured diffusion coefficient using FRAP. The specific parameters for each of these groups are detailed in Table 1. The groups consist of: 1) 2 % sodium alginate and 2 % agar, crosslinking without freezing – marked as 2 + 2 NF, 2) 2 % sodium alginate and 2 % agar, crosslinking after slow freezing (5°C/min) – marked as 2 + 2 SF, 3) 2 % sodium alginate and 2 % agar, crosslinking after rapid freezing (25°C/min) – marked as 2 + 2 RF, 4) 2 % sodium alginate and 0.5 % agar, crosslinking after slow freezing (5°C/min) – marked as 2 + 0.5 SF. The NF designation signifies the sample fabricated by 3D printing without freezing, serving as the control group in this study. The NF sample underwent crosslinking after printing on a 4 °C surface, without undergoing freezing. It is noteworthy that NF

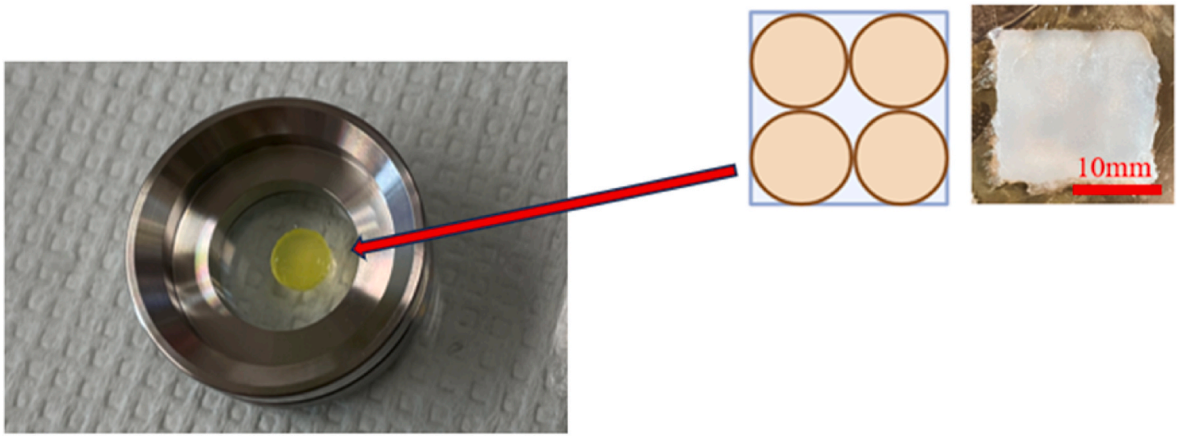

Fig. 2. Sample for FRAP Test. The figure depicts the sample used for the FRAP test. The test sample is depicted as a cylindrical shape with dimensions of 1 cm (diameter) by 1 mm (thickness). The sample was collected from the printed sample described earlier.

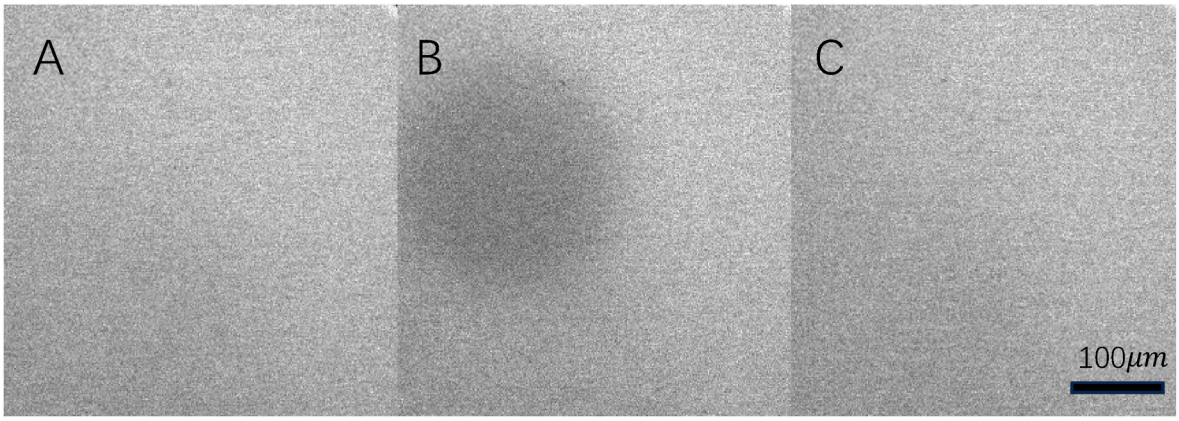

Fig. 3. Example of Fluorescent Images During Different Stages of FRAP Test. (A) Original fluorescent image at t = 0s (B) Initial laser bleach at t = 7.4s (C) Recovery image at t = 60s. The figure shows three images depicting different stages of the FRAP test. In image (A), the original fluorescent image at t = 0s is displayed. Image (B) illustrates the initial laser bleach occurring at t = 7.4s. Lastly, image (C) presents the recovery image observed at t = 60s.

Table 1
Each group is marked with a specific designation reflecting its composition and treatement method.

Experimental Group	Sodium Alginate (%)	Agar (%)	Freezing Rate	Crosslinking
2 + 2 NF	2	2	No freezing	Without freezing
2 + 2 SF	2	2	Slow (5°C/min)	During thawing
2 + 2 RF	2	2	Rapid (25 °C/min)	During thawing
2 + 0.5 SF	2	0.5	Slow (5°C/min)	During thawing

techniques are applicable to tissue engineering as well.

2.8. Scanning electron microscopy

Scanning electron microscopy (SEM) was performed on the samples using a Hitachi TM-4000 scanning electron microscope. Initially, the specimens were rapidly frozen in liquid nitrogen and subsequently subjected to freeze-drying in a 4.5 L, −50 °C freeze dryer (Labconco FreeZone) over a three-day period.

After collecting SEM images, we used ImageJ (NIH, US) to analyze the features of the pores. To estimate the pore size, we evaluated the average and standard deviation of 50–100 pores examined at three randomly chosen 1 cm diameter areas on the sample.

2.9. Statistical analysis

We utilized a one-way ANOVA followed by Duncan's multiple range test (DMRT) at a 95 % confidence level to compare the different experimental groups in terms of both AP and fluorescent recovery.

3. Result and discussion

3.1. Experimental samples

The study was conducted on a printed sample measuring 2 cm by 2 cm by 0.1 cm, which had undergone controlled directional solidification and crosslinking. Fig. 4 depicts a photograph of such a sample. The printing process remained consistent with that of previous research, as described in the preceding section [25].

3.2. Fluorescent recovery

First, we evaluated the fluorescent recovery in the bleached area. The fluorescent intensity recovery curves for various samples were plotted, as depicted in Fig. 5. To achieve a normalized recovery process, the equation below was utilized [30,31]:

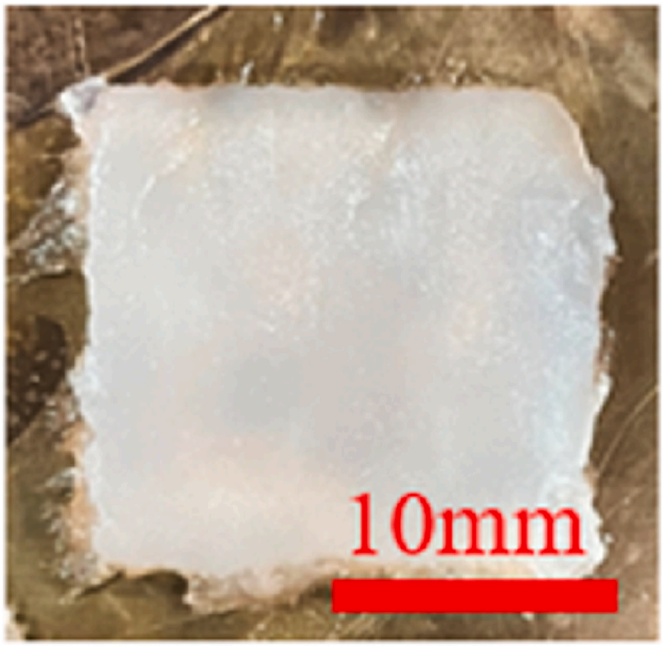

Fig. 4. illustrates the TCC printed sample (2 cm × 2 cm × 0.1 cm, Length × Width × Height).

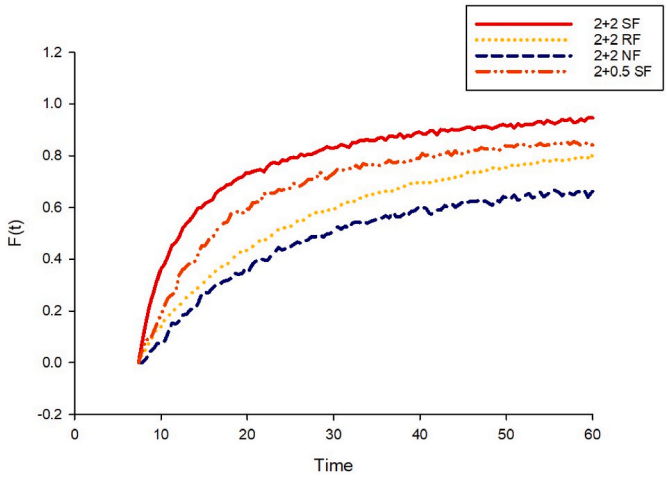

Fig. 5. illustrates the fluorescent signal recovery curve.

$$\overline{F}(t) = \frac{F(t) - F(0)}{F(\infty) - F(0)} \quad (1)$$

Here, the function F(t) represents the fluorescent intensity signal collected by the confocal microscope. A normalized fluorescent intensity signal was defined as $\overline{F}$ (t). F(0) represents the concentration of the fluorescent dye immediately after laser photobleaching, while F(∞) represents the fluorescent signal after full recovery, which we assume is equal to the fluorescent signal before the photobleaching, given that the bleach field is relatively small compared to the entire scaffold area.

It is evident from the data that the 2 + 2 SF group exhibits the fastest recovery compared to the 2 + 2 FF and 2 + 2 NF groups. This observation suggests that freezing can indeed influence the diffusion coefficient of the scaffold, and slow freezing may be a more effective method for enhancing the diffusion coefficient compared to rapid freezing. This finding bears significance in tissue engineering, as diffusion plays a pivotal role in bio-scaffolds, enabling essential biological transport processes such as the dispersion of oxygen, nutrients, and waste [2–4].

An explanation for this observation can be linked to the impact of cooling rates on the size of ice crystals. Previous research has demonstrated that in directional solidification, the size of ice crystals formed is directly correlated with the cooling rate during freezing and the speed at which the freezing interface advances, with higher cooling rates resulting in smaller ice crystals [7,32–37]. Upon melting, pores develop in the space previously occupied by the ice crystals. The mechanism of pore formation is associated with the inability of ice to incorporate solutes. Consequently, during freezing, solutes are expelled along the ice crystals, and upon melting, the imprint of the ice generates the pores [38–42]. Our earlier research has confirmed that the freezing process can increase the porosity of scaffolds [10,33]. Lower cooling rates produce larger ice crystals, and the findings of this study suggest that the diffusion coefficient in structures with larger pores is correspondingly larger. This outcome can be explained by the effect of tortuosity. The tortuosity in smaller pores bounded by the rejected solutes structure is greater. Other studies have also indicated a relationship between porosity and diffusion coefficient[41 42]. It's noteworthy that much earlier research in tissue engineering has employed freezing to create pores in engineered tissues [43–47]. These pores were deemed significant for cell growth, with pores larger than 100 μm being preferable [48]. Here we show that freezing rates influence porosity, and porosity affects two different aspects of tissue engineering: diffusivity and cell growth, which may be related.

3.3. Diffusion coefficient

The following Soumpasis equation was utilized to calculate the diffusion coefficient from the fluorescent recovery data [49].

$$D = 0.224 \frac{r_n^2}{\tau_{1/2}} \quad (2)$$

Where r_n is the radius of the bleach field and coefficient 0.224 was numerically determined [50]. $\tau_{1/2}$ is the half recovery time. Table 2 provides the values of the diffusion coefficient for different groups of samples.

Based on the recovery curve and the diffusion coefficient values, several interesting conclusions can be drawn:

1 Freezing has the capability to enhance the diffusion coefficient. This might be due to the ice crystals created by freezing, which can increase the porosity and consequently the diffusion coefficient of the scaffold.
2 Slow freezing proves to be more effective in improving the diffusion coefficient compared to rapid freezing. This may be attributed to the generation of larger ice crystals during slow freezing, resulting in larger pore sizes [25].
3 The concentration of agar has an effect on the diffusion coefficient of the scaffold. It seems that a higher concentration of agar, substantially reduces the variance in diffusion coefficient and allows for greater precision in designing a scaffold with a desirable diffusivity.

3.4. Scanning electron microscopy

Scanning electron microscopy (SEM) was employed to correlate the microstructural changes resulting from various TCC processes with the

Table 2
Diffusion coefficient value for different groups.

Sample Group	Diffusion coefficient (m^2s^{-1}) × 10^{-10}
2 + 2 SF	9.72 ± 4.50^{a}
2 + 0.5 SF	4.07 ± 1.65^{ab}
2 + 2 RF	2.40 ± 1.54^{b}
2 + 2 NF	1.62 ± 1.27^{b}

diffusivity characteristics of the printed samples. Fig. 6 illustrates electron microscope images of these tested samples.

The results obtained from electron microscopy (EM) reveal that samples subjected to directional solidification exhibit a directional pore structure, whereas those not subjected to freezing display a more homogeneous structure. Using Image J to analyze the features of the pores, as described earlier, we find that the 2 + 2 SF sample demonstrates a pore size of approximately 117 ± 30 μm, the 2 + 0.5 SF samples exhibit a directional pore size of around 43 ± 9 μm, while the 2 + 2 RF sample shows a pore size of approximately 25 ± 5 μm. The pore sizes exhibit a significant difference among the three groups ($p < 0.05$). From the SEM results, it is evident that samples prepared with lower concentrations of agar display a more aligned microstructure. This observation suggests a role for agar during the printing process. As discussed in our previous research [25], agar functions during the TCC process to stabilize the sodium alginate before crosslinking, thereby enhancing TCC printing precision on a macro level. However, an increase in agar concentration also appears to influence the microstructure during directional solidification. Compared to the SF group, the RF groups exhibit lesser directionality in the microstructures, possible because of supercooling and ice nucleation ahead of the ice front.

The fundamental mechanism governing diffusion primarily arises from random molecular motion. In unobstructed spaces, particles tend to move isotropically, but their motion can be influenced by barriers within the space. The electron microscope images suggest that scaffolds made by directional freezing will have anisotrotropic diffusivity. Previous studies conducted by Travascio et al. [51] using FRAP on bovine annulus fibrosus and bovine meniscus have suggested that anisotropic structures within tissues can lead to anisotropic diffusion. In the upcoming section, we assess the anisotropic diffusion in the scaffolds of this study.

3.5. Anisotropic diffusion

Anisotropic diffusivity is a prevalent characteristic of biological tissues, commonly observed in tissues such as cartilage, ligaments, and intervertebral discs, resulting in anisotropic diffusion within these structures [51,52]. Despite this, there has been limited research focused on developing bio-scaffolds with controlled anisotropic diffusivity. In this section, we assess the anisotropic diffusion properties of the TCC-printed sample.

Directional solidification possesses the capability to generate controlled anisotropic microstructures. Scaffolds produced through directional solidification often display directional pore structures. By adjusting the freezing rate, it becomes possible to create anisotropic microstructures of varying dimensions [7–10,19,33]. We hypothesize that such anisotropic structures may yield anisotropic diffusion. In this study, we employed FRAP to confirm the presence of anisotropic diffusion phenomena in the scaffolds fabricated via directional solidification.

Based on the directional solidification parameters and the SEM results, we hypothesized that the most notable disparity in diffusion recovery arises when the angle between the measured diffusion direction is 90°. We designated the diffusion coefficients along two principal directions as D_x and D_y. To discern the orientation of the diffusion tensor, we devised a directional detection algorithm.

The algorithm operates as follows: detection masks, depicted in Fig. 7, were designed. The outer large circle represented the bleached field, with its center defined as the origin. Two smaller inner circles, labeled as 1 and 2, served as mask circles for identifying D_x and D_y. We systematically rotated the axis from 0 to 180° in 2° increments, based on the origin of the bleaching large circle. Throughout this rotation process, we recorded the difference between the normalized recovery F(t) calculated using the two small masks. The F(t) value was computed at t = 30s. Upon observing the largest difference ΔF, we recorded the rotation angle θ. Subsequently, we rotated the original axis by θ to establish a new coordinate system. D_x (x-direction diffusion) and D_y (y-direction diffusion) were then computed based on this new coordinate system from masks 1 and 2 (Fig. 7 illustrates the rotation process).

In instances of isotropic diffusion, the recovery process for both mask circle 1 and mask circle 2 should be similar, leading to no significant difference between the values of F for mask 1 and 2. However, in an anisotropic scenario, the values of F for mask circle 1 and mask circle 2 could differ due to anisotropic diffusion.

D_x and D_y were computed using the same method as described in equation (2). However, because the bleach fields for mask circle 1 and 2

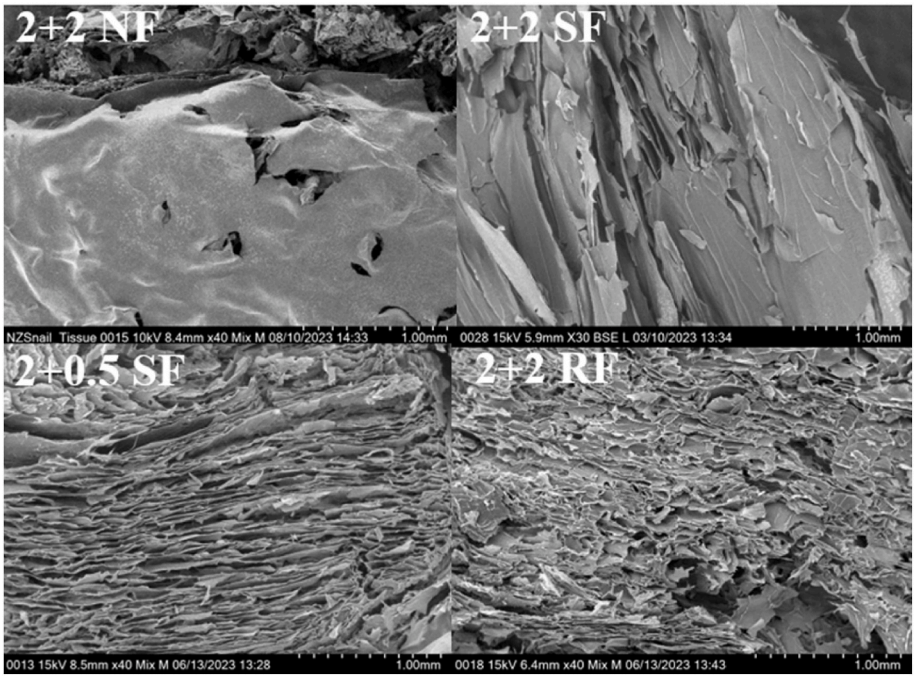

Fig. 6. Shows electron microscope images of the tested samples.

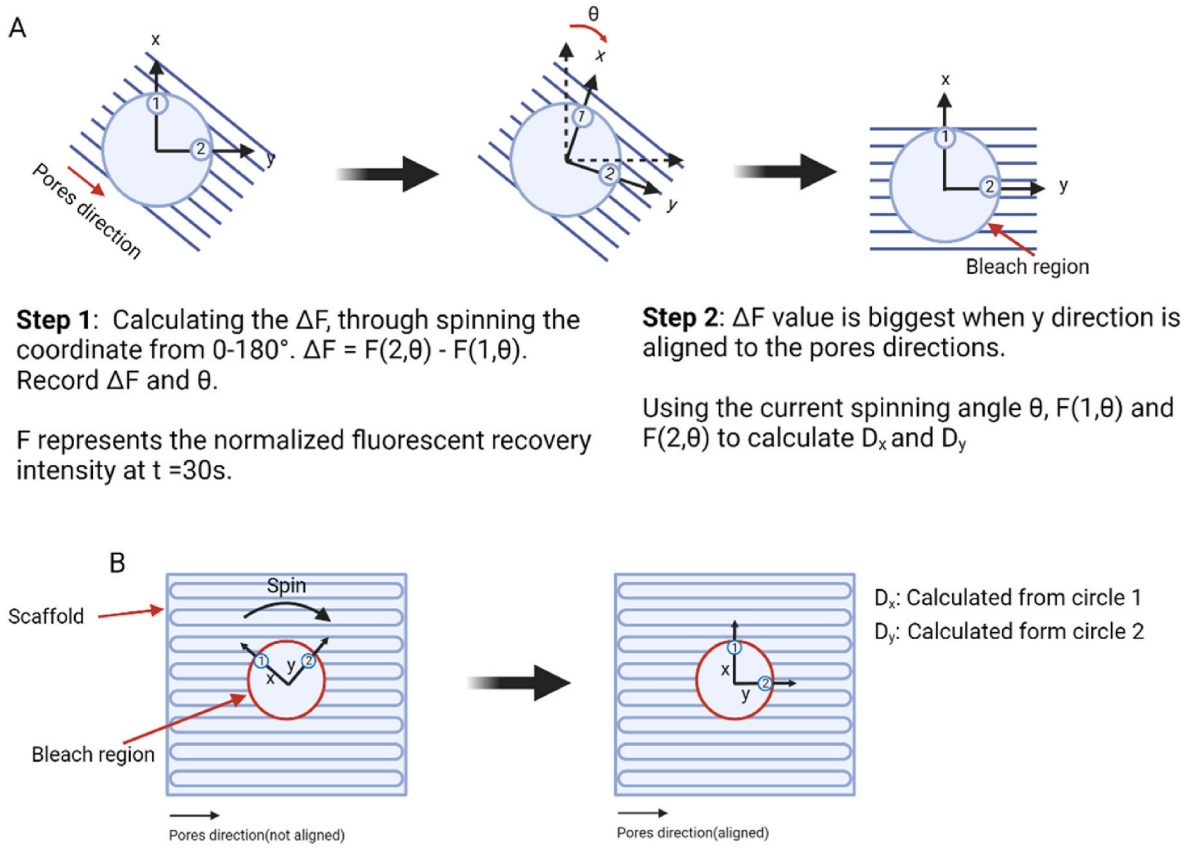

Fig. 7. Direction Detector. (A) The steps of the direction detection. (B) Illustration of the image spinning process in a printed scaffold.

are sub-fields within the larger outer bleach field, the absolute diffusion coefficient values D_x and D_y may contain some errors. Instead of directly presenting the values of D_x and D_y, we introduced a parameter called the relative anisotropic level (AL) to evaluate the degree of anisotropy. The AL was defined using the following equation:

$$AL = \frac{D_x}{D_y} \tag{3}$$

The x-direction diffusion coefficient, denoted as D_x, and the y-direction diffusion coefficient, denoted as D_y, are defined as follows: the y-direction represents the higher recovery direction, hence $D_x < D_y$ for all cases, and, $0 < AL < 1$ is always satisfied. We evaluate the error by measuring multiple repetitions of AL. Fig. 8 shows that in the NF sample

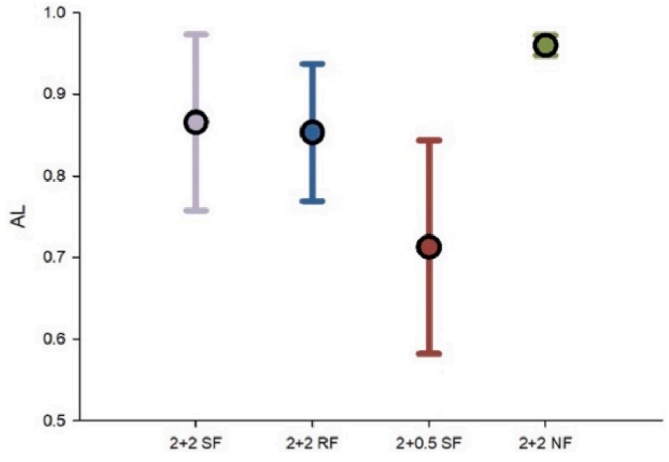

Fig. 8. AL value for different groups.

the AL is close to 1, i.e. isotropic diffusivity, whereas for the directional solidification cases the AL indicates anisotropy.

4. Conclusion

TCC is a novel 3D bioprinting technique targeting the printing of large and complex scaffolds. One aspect of printing complex structures is controlling the diffusion coefficient of the printed scaffolds. Fluorescence Recovery After Photobleaching (FRAP) is a widely used method for analyzing the movement of molecules within tissues. We utilized TCC and FRAP to print scaffolds and evaluate their diffusion coefficient. Our results indicated that it is possible to utilize TCC to print scaffolds with modified diffusion coefficients without changing the component concentration. The data shows that with an ink mixture of 2 % sodium alginate and 2 % agar, it is possible to print scaffolds with a relatively low diffusion coefficient (1.62 ± 1.27 $(m^2 s^{-1})$ $\times$ 10^{-10})using a rapid freezing rate and scaffolds with a high diffusion coefficient (9.72 ± 4.50 $(m^2 s^{-1})$ $\times$ 10^{-10}) using a slow freezing rate. This indicates that the freezing rate can be used as an input parameter to modify the diffusion coefficient of scaffolds while maintaining the same components.

Another finding in this paper is that TCC technology can also print scaffolds with anisotropic diffusion coefficients. We introduced a parameter called the anisotropic percentage to evaluate the anisotropic diffusion and used SEM to reverify the result. An algorithm was also designed to detect the directional diffusion angle, showing that the level of anisotropy can also be related to the freezing rate. Our results also showed that the concentration of agar has an influence on the diffusion coefficient of the scaffold. This may be due to agar's influence on ice crystal size during freezing. We hope our results can be used for further development of complex cell scaffolds that better mimic real tissues in the body. Further studies can be conducted with printed scaffolds with embedded cells to test cell proliferation based on the anisotropic

structure.

Funding

This research was funded by the NSF Engineering Research Center for Advanced Technologies for Preservation of Biological Systems (ATP-Bio) NSF EEC#1941543.

Institutional review board statement

Not applicable.

Informed consent statement

Not applicable.

CRediT authorship contribution statement

Leo Lou: Writing – original draft, Visualization, Validation, Software, Methodology, Investigation, Data curation. **Boris Rubinsky:** Writing – review & editing, Supervision, Resources, Project administration, Methodology, Investigation, Funding acquisition, Conceptualization.

Declaration of competing interest

The authors declare the following financial interests/personal relationships which may be considered as potential competing interests: Boris Rubinsky has patent ##US2022016827A1 issued to THE REGENTS OF THE UNIVERSITY OF CALIFORNIA. If there are other authors, they declare that they have no known competing financial interests or personal relationships that could have appeared to influence the work reported in this paper.

Data availability

Data will be made available on request.

Acknowledgement

We have used Chat GPT to improve the English in the write-up. Every statement generated by ChatGPT was verified for accuracy.

References

[1] C.M. Agrawal, R.B. Ray, Biodegradable polymeric scaffolds for musculoskeletal tissue engineering, J Biomed Matt Res 55 (2) (2001) 141–150, https://doi.org/10.1002/1097-4636(200105)55:2%3C141::aid-jbm1000%3E3.0.co;2-j.
[2] J. Yang, G. Shi, J. Bei, et al., Fabrication and surface modification of macroporous poly(L-lactic acid) and poly(L-lactic-co-glycolic acid) (70/30) cell scaffolds for human skin fibroblast cell culture, J.of Biomed Mat Res 62 (3) (2002) 438–446, https://doi.org/10.1002/jbm.10318.
[3] G.S. Offedu, L. Mohee, R.E. Cameron, Scale and structure dependent solute diffusivity within microporous tissue engineering scaffolds, J. Mater. Sci. Mater. Med. 31 (5) (2020) 46.
[4] B. Cai, D. Kilian, Mejia D. Ramos, et al., Diffusion-based 3D bioprinting Strategies, Adv. Sci. 11 (8) (2024) e2306470, https://doi.org/10.1002/advs.202306470.
[5] M. Adamkiewicz, B. Rubinsky, Cryogenic 3D printing for tissue engineering, Cryobiology 71 (3) (2015) 518–521, https://doi.org/10.1016/j.cryobiol.2015.10.152.
[6] B. Rubinsky, Adamkievicz Michal, Z. Shaked, System aparatus and methods for cryogenic 3D printing, US Patent 11 (584) (2023) 66.
[7] G. Ukpai, B. Rubinsky, A mathematical analysis of directional solidification of aqueous solutions, J. Heat Tran. 142 (2) (2020) 22401, https://doi.org/10.1115/1.4045312, 1.
[8] G. Ukpai, B. Rubinsky, A three-dimensional model for analysis and control of phase change phenomena during 3D printing of biological tissue, Bioprinting 18 (2020) e00077, https://doi.org/10.1016/j.bprint.2020.e00077.
[9] J.A. Preciado, P. Skandakumaran, S. Cohen, et al., Utilization of directional freezing for the construction of tissue engineering scaffolds, Heat Transfer 4 (2003) 439–442, https://doi.org/10.1115/IMECE2003-42067.
[10] L. Warburton, L. Lou, B. Rubinsky, A modular three dimensional bioprinter for printing porous scaffolds for tissue engineering, Journal of Heat Transfer; ASME Trans 144 (2022) 31205, https://doi.org/10.1115/1.4053198, 1.
[11] B. Zawada, G. Ukpai, M.J. Powell-Palm, et al., Multi-layer cryolithography for additive manufacturing, Progress in Additive Manufacturing 3 (4) (2018) 245–255, https://doi.org/10.1007/s40964-018-0045-3.
[12] G. Ukpai, J. Sahyoun, R. Stuart, et al., A parallel multiple layer cryolithography device for the manufacture of biological material for tissue engineering, Journal of Medical Devices, Transactions of the ASME 13 (3) (2019), https://doi.org/10.1115/1.4043080, 035001–1.
[13] W. Zhang, M.C.M. Leu, Z. Ji, et al., Rapid freezing prototyping with water, Mater. Des. 20 (2–3) (1999) 139–145.
[14] G. Kim, S. Ahn, H. Yoon, et al., A cryogenic direct-plotting system for fabrication of 3D collagen scaffolds for tissue engineering, J. Mater. Chem. 19 (46) (2009) 881–887, https://doi.org/10.1039/b914187a.
[15] Z.C. Tan, C. Parisi, L. Di Silvio, et al., Cryogenic 3D printing of super soft hydrogels, Sci. Rep. 7 (1) (2017) 16293, https://doi.org/10.1038/s41598-017-16668-9.
[16] Z. Xiong, Y.N. Yan, S.G. Wang, et al., Fabrication of porous scaffolds for bone tissue engineering via low-temperature deposition, Scripta Mater. 46 (11) (2002) 771–776, https://doi.org/10.1016/S1359-6462(02)00071-4.
[17] C. Wang, Q. Zhao, M. Wang, Cryogenic 3D printing for producing hierarchical porous and rhBMP-2-loaded Ca-P/PLLA nanocomposite scaffolds for bone tissue engineering, Biofabrication 9 (2) (2017) 025031, https://doi.org/10.1088/1758-5090/aa71c9.
[18] A. Kumar, R.A. Brown, D.B. Roufaeil, et al., DeepFreeze 3D-biofabrication for bioengineering and storage of stem cells in thick and large-scale human tissue analogs, Adv. Sci. 6 (2024) e2306683, https://doi.org/10.1002/advs.202306683. Jan.
[19] L. Warburton, B. Rubinsky, Freezing modulated crosslinking: a crosslinking approach for 3D cryoprinting, Bioprinting 27 (2022) e00225, https://doi.org/10.1016/j.bprint.2022.e00225.
[20] L. Warburton, B. Rubinsky, Cryopreservation of 3D bioprinted scaffolds with temperature-controlled-cryoprinting, Gels 9 (6) (2023) 9060502, https://doi.org/10.3390/gels9060502.
[21] Y. Zhao, M.J. Powell-Palm, G. Ukpai, et al., Phase change interface stability during isochoric solidification of an aqueous solution, Appl. Phys. Lett. 117 (13) (2020), https://doi.org/10.1063/5.0019878.
[22] L. Lou, C. Bilbao-Sainz, D. Wood, et al., Temperature controlled cryoprinting of food for dysphagia patients, Innovative Food Sci. Emerging Technol. 86 (2023) 103362, https://doi.org/10.1016/j.ifset.2023.103362.
[23] E. Axpe, M.L. Oyen, Applications of alginate-based bioinks in 3D bioprinting, Int. J. Mol. Sci. 17 (2016) 17121976, https://doi.org/10.3990/ijms121976.
[24] A.D. Augst, H.J. Kong, D.J. Mooney, Alginate hydrogels as biomaterials, Macromol. Biosci. (2006), https://doi.org/10.1002/mabi.200600069.
[25] L. Lou, B. Rubinsky, Temperature-controlled 3D cryoprinting inks made of mixtures of alginate and agar, Gels 9 (2023) 689, https://doi.org/10.3390/gels9090689.
[26] E.W. Skinner, E.N. Cooper, F.E. Beck, Reversible and irreversible hydrocolloid impression materials, J. Am. Dent. Assoc. 40 (2) (1950) 196–207, https://doi.org/10.14219/jada.archive.1950.0029.
[27] Z.-C. Yin, Y.-L. Wang, K. Wang, A pH-responsive composite hydrogel beads based on agar and alginate for oral drug delivery, J. Drug Deliv. Sci. Technol. 43 (2018) 12–18.
[28] J. Wang, Y. Liu, X. Zhang, et al., 3D printed agar/calcium alginate hydrogels with high shape fidelity and tailorable mechanical properties, Polymer (Guildf) 214 (2021) 13238.
[29] M. Carnell, A. Macmillan, R. Whan, Fluorescence recovery after photobleaching (FRAP): acquisition, analysis, and applications, Methods Mol. Biol. 1232 (2015) 255–271, https://doi.org/10.1007/978-1-4939-1752-5_18.
[30] D. Axelrod, D.E. Koppel, J. Schlessinger, et al., Mobility measurement by analysis of fluorescence photobleaching recovery kinetics, Biophys. J. 16 (9) (1976) 1055–1069, https://doi.org/10.1016/S0006-3495(76)85755-4.
[31] J. Yguerabide, J.A. Schmidt, E.E. Yguerabide, Lateral mobility in membranes as detected by fluorescence recovery after photobleaching, Biophys. J. 40 (1) (1982) 69–75, https://doi.org/10.1016/S0006-3495(82)84459-7.
[32] B. Rubinsky, Directional solidification for the controlled freezing of biomaterials, US Patent 4 (531) (1985) 373.
[33] B. Rubinsky, M. Ikeda, A cryomicroscope using directional solidification for the controlled freezing of biological material, Cryobiology 22 (1) (1985) 55–68, https://doi.org/10.1016/0011-2240(85)90008-2.
[34] H. Ishiguro, B. Rubinsky, Mechanical interactions between ice crystals and red blood cells during directional solidification, Cryobiology 31 (5) (1994) 483–500, https://doi.org/10.1006/cryo.1994.1059.
[35] C. Stolze, T. Janoschka, U.S. Schubert, et al., Directional solidification with constant ice front velocity in the ice-templating process, Adv. Eng. Mater. (2016), https://doi.org/10.1002/adem.201500235.
[36] Q. Xu, H. Zhang, X. Qi, et al., Multiscale modeling and simulation of directional solidification process of turbine blade casting with MCA method, Metall. Mater. Trans. B 45 (2) (2014) 555–561, https://doi.org/10.1007/s11663-013-9909-6.
[37] H. Ishiguro, B. Rubinsky, Microscopic behavior of ice crystals and biological cells during directional solidification of solutions with cells, Transactions of the Japan Society of Mechanical Engineers Series B 60 (572) (2011) 1349–1355, https://doi.org/10.1299/kikaib.60.1349.
[38] H.L. Tsai, B. Rubinsky, A “front tracking” finite element study on change of phase interface stability during solidification processes in solutions, J. Cryst. Growth 70 (1–2) (1984) 56–63, https://doi.org/10.1016/0022-0248(84)90247-1.

[39] H.L. Tsai, B. Rubinsky, A numerical study using “front tracking” finite elements on the morphological stability of a planar interface during transient solidification processes, J. Cryst. Growth 69 (1) (1984) 29–46, https://doi.org/10.1016/0022-0248(84)90006-X.
[40] B. Rubinsky, Solidification processes in saline solutions, J. Cryst. Growth 62 (3) (1983) 513–522, https://doi.org/10.1016/0022-0248(83)90394-9.
[41] Q.L. Loh, C. Choong, Three-Dimensional scaffolds for tissue engineering applications: role of porosity and pore size, Tissue Engineering Part B-Reviews 19 (6) (2013) 485–502, https://doi.org/10.1089/ten.teb.2012.0437.
[42] P. Yadav, G. Beniwal, K. Saxena, A review on pore and porosity in tissue engineering, Mater. Today 44 (1) (2021) 2623–2628, https://doi.org/10.1016/j.matpr.2020.12.661.
[43] F.J. O’Brien, B.A. Harley, I.V. Yannas, et al., Influence of freezing rate on pore structure in freeze-dried collagen-GAG scaffolds, Biomaterials 25 (6) (2004) 1077–1086, https://doi.org/10.1016/s0142-9612(03)00630-6.
[44] I.V. Yannas, D.P. Orgill, J.F. Burke, Template for skin regeneration, Plast. Reconstr. Surg. 127 (1) (2011) 60S–70S, https://doi.org/10.1097/PRS.0b013e318200a44d.
[45] N. Dagalakis, J. Flink, P. Stasikelis, et al., Design of an artificial skin. Part III. Control of pore structure, J. Biomed. Mater. Res. 14 (4) (1980) 511–528, https://doi.org/10.1002/jbm.820140417.
[46] F.J. O’Brien, B.A. Harley, I.V. Yannas, et al., Influence of freezing rate on pore structure in freeze-dried collagen-GAG scaffolds, Biomaterials 25 (6) (2004) 1077–1086, https://doi.org/10.1016/s0142-9612(03)00630-6.
[47] H.M. Loree, I.V. Yannas, B. Mikic, et al., Freeze-drying process for fabrication of polymeric bridges for peripheral nerve regeneration, in: Bioengineering, Proceedings of the Northeast Conference, 1989.
[48] I.V. Yannas, J.F. Burke, Design of an artificial SKIN .1. Basic design principles, J. Biomed. Mater. Res. 14 (1) (1980) 65–81, https://doi.org/10.1002/jbm.820140108.
[49] M. Kang, C.A. Day, A.K. Kenworthy, E. DiBenedetto, Simplified equation to extract diffusion coefficients from confocal FRAP data, Traffic 13 (12) (2012) 1589–1600.
[50] D. Soumpasis, Theoretical analysis of fluorescence photobleaching recovery experiments, Biophys. J. 41 (1) (1983) 95–97.
[51] L. Filidoro, O. Dietrich, J. Weber, et al., High-resolution diffusion tensor imaging of human patellar cartilage: feasibility and preliminary findings, Magn. Reson. Med. 53 (5) (2005) 993–998, https://doi.org/10.1002/mrm.20469.
[52] F. Travascio, W. Zhao, W.Y. Gu, Characterization of anisotropic diffusion tensor of solute in tissue by video-FRAP imaging technique, Ann. Biomed. Eng. 37 (4) (2009) 813–823, https://doi.org/10.1007/s10439-009-9655-8.